BMC Veterinary Research

RESEARCH

Open Access

Transcriptome analysis reveals the mechanism of Rhodiola polysaccharide affecting the proliferation of porcine Leydig cells under hypoxia

Jinting Luo[1], Lei Wang[1], Youli Yao[1], Xuan Luo[1], Jianbo Zhang[1], Dandan Luo[1], Tian Tian[1] and Guofang Wu[1*]

Abstract

Hypoxia can affect the function of the male reproductive system and reduce fertility. Rhodiola polysaccharide (RDP) is the active ingredient of *Rhodiola rosea L.* and has a positive effect on reproductive cells. However, the mechanism of the effect of RDP on the proliferation of cells under hypoxia is still unclear. The experiment selected porcine Leydig cells (PLCs) as the test object and divided them into three groups: normal group, hypoxia group, and hypoxia + RDP-treated group. Cell viability was detected using CCK8 assay. RNA-Seq technology was used to identify the key genes that influence the effect of RDP on PLCs under hypoxia conditions and to determine their regulatory pathways. Transcriptome sequencing of PLCs from the N and H groups identified 6,794 differentially expressed genes (DEGs), including 3,329 up-regulated genes and 3,465 down-regulated genes. These DEGs were significantly enriched in the cell cycle signaling pathway, indicating that hypoxia mainly affects the cell cycle and inhibits cell proliferation. Furthermore, comparison of the transcriptomes between the H and HR group revealed 285 DEGs, including 137 up-regulated and 148 down-regulated, most of DEGs were found to be enriched in oxidative phosphorylation pathways. RDP inhibits PLCs apoptosis and promotes cell proliferation by up-regulating the expression of *CXCL2*, *JUNB* and *VCAM1* of the TNF signaling pathway, and *VEGFA*, *SGK2* and *SPP1* of the PI3K/AKT signaling pathway. These genes deserve further study as candidate for understanding the role of RDP in alleviating the hypoxia stress.

Keywords Candidate genes, Hypoxia, Porcine Leydig cells, Rhodiola polysaccharide, RNA-seq

*Correspondence:
Guofang Wu
qhdxwuguofang@126.com
[1]Plateau Livestock Genetic Resources Protection and Innovative Utilization Key Laboratory of Qinghai Province, Academy of Animal Science and Veterinary, Qinghai University, Xining 810016, China

Introduction

Oxygen is essential for all animals' life, and hypoxia, a prominent feature of plateau environments, poses significant challenges to for introduced livestock [1]. The lack of oxygen supply will make the body produce a lot of ROS and redox system imbalance, leading to animal physiological dysfunction [2–3]. The simulated hypoxic conditions in vitro may cause damage to testicular reproductive function in rats by inducing germ cell apoptosis [4]. Leydig cells are one of the important reproductive cells, and their normal growth is crucial to male fertility and reproductive health [5]. Hypoxia can lead to reduced viability of Leydig cells [6]. Therefore, there is an urgent need to explore or discover drugs that can protect reproductive function in hypoxia conditions.

Chinese herbal medicine is rich in resources and ingredients [7]. *Rhodiola rosea L.*, as one of the traditional Tibetan medicines, has been proven to play an anti-hypoxia role by alleviating oxidative stress, inhibiting the expression of inflammatory factors, and inhibiting cell apoptosis [8–9]. The active component RDP (Rhodiola polysaccharide) is known to promote cellular proliferation [10–12]. At the same time, previous studies have found that adding RDP to the culture can significantly improve the cell viability of porcine Leydig cells (PLCs) under hypoxia [13]. Based on these findings, we hypothesized that RDP could protect Leydig cells from hypoxia-induced damage through specific molecular pathways. The primary objective of this research is to elucidate the mechanisms through which RDP alleviates hypoxia stress in Leydig cells by conducting transcriptome sequencing and identifying relevant candidate genes involved in these pathways.

Results

Effect of RDP on cell viability from PLCs under hypoxia

Figure 1 showed that the cell viability of H group was significantly reduced compared to that in N group ($p < 0.05$). Conversely, HR group cell viability was significantly higher than that of H group ($p < 0.05$), close to the level of N group ($p > 0.05$).

Different letters indicate significant difference ($p < 0.05$), while the same letters indicate no significant difference ($p > 0.05$). N: normal group; H: hypoxia group; HR: hypoxia + RDP group.

Quality analysis of RNA-Seq data

Following sequencing on the Illumina platform, the initial reads varied from 41,118,714 to 51,529,512 (Table 1). As can be seen from the table, the GC content in each group is higher than 51%, and the Q30 is above 93%, indicating that the sequencing quality is good and can be used for subsequent analysis.

Sequencing data comparison and analysis

The clean reads were aligned with the pig reference genome to generate the mapped reads (Table 2). The total number of reads across all 9 samples exceeded 41,000,000. The overall mapping rate was greater than 93%, with the proportion of multiple mappings ranging from 2 to 4%, and the unique mapping rate approximately 90%.

Differentially expressed genes analysis

Differentially expressed genes (DEGs) were identified through digital gene expression tags. The analysis revealed that 6,794 DEGs (Fig. 2A and Supplementary Table 1), 7,799 DEGs (Fig. 2B and Supplementary Table 2), and 285 DEGs (Fig. 2C and Supplementary Table 3) were detected in the PLCs for the comparisons H vs. N, HR vs. N, and HR vs. H, respectively (with FC > 1.2 and FDR < 0.02). Notably, the number of DEGs between the N group and the H group was significantly higher compared to the comparison between the H group and the HR group (Fig. 2D).

Functional analysis of DEGs in PLCs under different oxygen conditions

To further investigate the role of these DEGs under hypoxia conditions, we conducted GO and KEGG analyses to assess their functional implications. The GO annotation results revealed that 6,794 DEGs in the H vs. N comparison were significantly enriched in 9 cellular components (CC) and 11 molecular functions (MFs). Key functions identified include nucleotide binding (GO: 0000166), nucleoside phosphate binding (GO: 1901265), and small molecule binding (GO: 0036094) (Fig. 3A and Supplementary Table 4). Furthermore, the DEGs were mapped to 332 pathways, with 59 showing significant enrichment ($p < 0.05$). Notable enriched pathways included the cell cycle (ssc04110) and DNA replication (ssc03030), among others (Fig. 3B and Supplementary Table 5).

Functional analysis of DEGs in PLCs by RDP under hypoxia

To further explore the impact of DEGs on RDP in PLCs under hypoxia conditions, a KEGG pathway enrichment analysis and GO functional annotation were performed on 285 DEGs. GO enrichment analysis revealed that these DEGs were primarily involved in processes such as epithelial cell proliferation (GO: 0010631), tissue migration (GO: 0090130), and epithelium migration (GO: 0090132) (Fig. 4A and Supplementary Table 6). KEGG pathway enrichment for the DEGs in the HR vs. H comparison identified 241 pathways (Fig. 4B and Supplementary Table 7), with the Prion disease pathway showing the most significant enrichment ($p < 0.01$). Additionally, the TNF signaling pathway and PI3K-Akt signaling pathway,

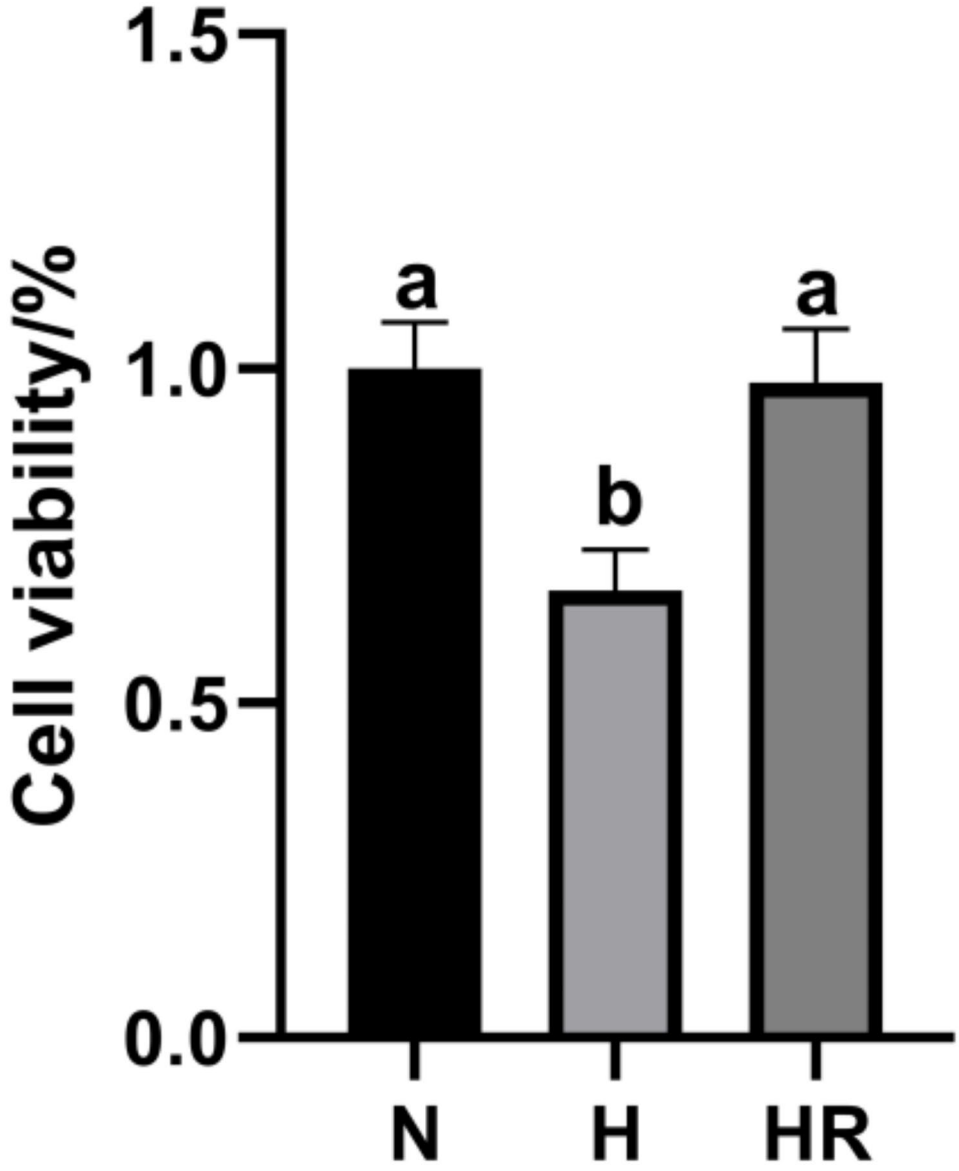

Fig. 1 Effect of RDP on cell viability in PLCs under hypoxia

Table 1 Statistics of mRNA sequencing data

Sample	Raw Reads	Clean Reads	Error rate(%)	Q20(%)	Q30(%)	GC content(%)
N_1	51,529,512	50,628,908	0.03	97.71	93.69	52.05
N_2	41,118,714	40,000,220	0.03	97.45	93.06	51.15
N_3	48,005,902	47,146,328	0.03	97.46	93.1	52.91
H_1	44,616,296	43,793,886	0.03	97.63	93.5	52.27
H_2	46,067,774	45,222,724	0.03	97.81	93.96	52.71
H_3	50,402,852	49,643,294	0.03	97.52	93.2	53.51
HR_1	49,326,384	48,554,300	0.03	97.93	94.17	53.02
HR_2	42,845,080	41,637,802	0.03	97.7	93.73	52.61
HR_3	46,982,818	46,013,430	0.02	97.98	94.33	53.47

Table 2 mRNA sequence alignment results

Sample	Total reads	Total mapped	Multiple mapped	Unique mapped
N_1	50,628,908	48,041,121(94.89%)	1,474,900(2.91%)	46,566,221(91.98%)
N_2	40,000,220	37,570,412(93.93%)	1,175,485(2.94%)	36,394,927(90.99%)
N_3	47,146,328	44,809,710(95.04%)	1,414,098(3.0%)	43,395,612(92.04%)
H_1	43,793,886	41,336,968(94.39%)	1,284,480(2.93%)	40,052,488(91.46%)
H_2	45,222,724	42,780,896(94.6%)	1,353,602(2.99%)	41,427,294(91.61%)
H_3	49,643,294	47,102,859(94.88%)	1,506,148(3.03%)	45,596,711(91.85%)
HR_1	48,554,300	46,114,069(94.97%)	1,473,098(3.03%)	44,640,971(91.94%)
HR_2	41,637,802	39,468,067(94.79%)	1,295,059(3.11%)	38,173,008(91.68%)
HR_3	46,013,430	43,457,092(94.44%)	1,597,458(3.47%)	41,859,634(90.97%)

both associated with cell proliferation and apoptosis, were notably enriched among the DEGs.

qRT-PCR verification results

The qRT-PCR was performed in order to verify the results from transcriptome sequencing for 5 DEGs. The qRT-PCR results of five genes are shown in Fig. 5 and the expression of target genes between the three groups was consistent with the RNA-seq results, indicative of the reliability of the transcriptome sequencing results.

Discussion

Research shows that hypoxia accelerates the formation of reactive oxygen species (ROS) in cells, leading to potential cell damage and inhibiting cell proliferation [14–15]. Study results demonstrate that the cell viability of PLCs cultured under hypoxia is significantly lower than that of cells cultured under normal conditions, suggesting that hypoxia inhibits cell proliferation. KEGG analysis showed that the differentially expressed genes (DEGs) were enriched in pathways related to the cell cycle, DNA replication, and cell senescence. The KEGG pathway most significantly enriched by DEGs was the cell cycle pathway. The regulation of cell cycle is a highly complex process involving multiple signaling pathways and cytokines [16]. Under normal physiological conditions, precise control of the cell cycle is essential for maintaining tissue homeostasis and facilitating damage repair [17]. However, when this signaling pathway is mutated or dysregulated, cell proliferation is inhibited, leading to reduced cell viability [18]. Hypoxia usually modulates key cell cycle-related genes, such as cyclins, cyclin-dependent kinases (CDKs), and cell cycle-dependent kinase inhibitors, by altering multiple intracellular signaling pathways [19–20]. These genes play key roles in different stages of the cell cycle, ensuring the smooth transition of cells from the G1 phase to the S phase, G2 phase, and M phase, to ensure that cells enter and pass through different cell cycle stages at the appropriate time, thus maintaining normal cell proliferation [21–22]. In this study, hypoxia regulated various stages of the cell cycle by altering the expression of cell cycle-related genes, thereby inhibiting cell proliferation. Specifically, hypoxia affects cell cycle progression by down-regulating the expression of cell division cyclins (*CCNB1*, *CCNA2*, *CCNB2*, *CCNE2*, *CCND1*, *CCNE1*, *CCNB3*, *CCND2*), inhibiting the activity of CDKs (*CDK1*, *CDK2*, *CDK4*, *CDK6*), and upregulating the expression of cell cycle-dependent kinase inhibitors (*CDKN1C*, *CDKN2C*, *CDKN2B*), thus affecting cell vitality.

RDP, a major bioactive ingredient extracted from *Rhodiola rosea L.*, exhibits significant antioxidant and anti-inflammatory properties [23]. In this study, we found that RDP protects the viability of PLCs under hypoxia conditions through modulation of key cellular processes including energy metabolism, proliferation, and survival under oxidative stress. To explore the underlying molecular mechanisms, we identified 285 differentially expressed genes (DEGs) between the hypoxia (H) and hypoxia + RDP (HR) groups. Our analysis revealed that RDP exerts its protective effects primarily through two major signaling pathways: the TNF/NF-κB pathway and the PI3K/AKT pathway. These signaling pathways are closely related to cell proliferation and apoptosis [24–26]. Among the identified DEGs, *VCAM1* (vascular cell adhesion molecule 1), *JUNB* (Recombinant Jun B Proto Oncogene) and *CXCL2* (CXC Chemokine Ligand 2) were significantly up-regulated in the HR group and enriched in both TNF signaling and NF-kappa B signaling pathways. *VCAM1*, an important adhesion molecule, facilitates cell interactions and co-localization [27–28]. *JUNB*, a component of the Activator Protein-1 (AP-1) transcription factor, promotes cell proliferation and inhibits apoptosis [29–30]. *CXCL2*, a chemokine, stimulates proliferation primarily through AKT activation [31]. The up-regulation of these genes suggests their involvement in RDP-mediated cell proliferation and survival.

Furthermore, we found that RDP significantly modulates the PI3K/AKT signaling pathway, which is crucial for cell growth, proliferation and survival [32–33]. Key downstream effector molecules of this pathway, including *VEGFA*, *SGK2*, and *SPP1*, were notably up-regulated in the HR group. *VEGFA* promotes cell survival, inhibits apoptosis, and supports cell proliferation through its receptor signaling pathway, particularly via PI3K/Akt

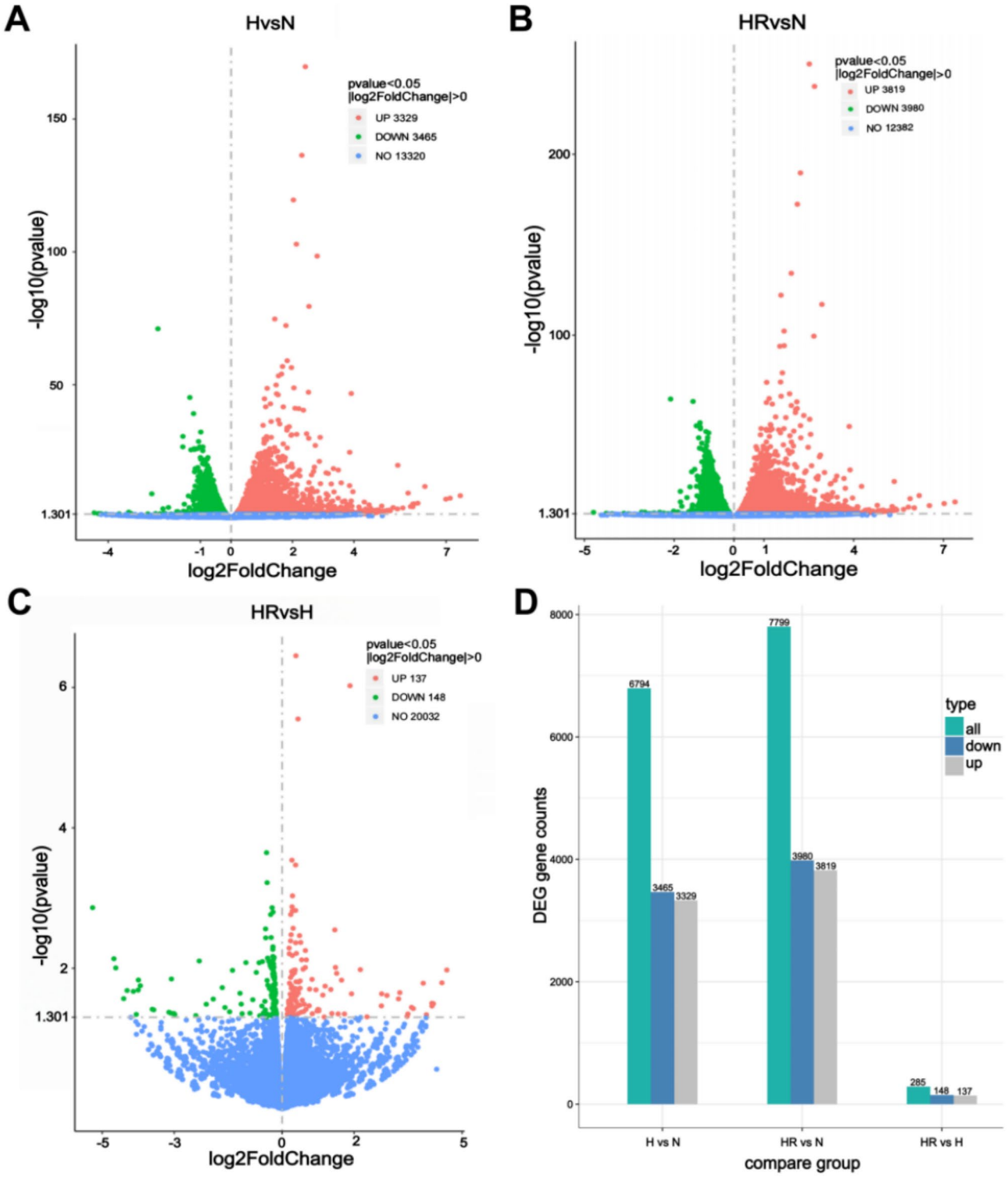

Fig. 2 Differentially expressed genes analysis
(**A-C**) Analysis of the volcano plot of DEGs. Upregulated genes are shown in red, down-regulated genes are own in green, and genes with no significant difference in expression are indicated in blue, significance was indicated by $p < 0.05$. (**D**) DEGs statistics in the each group.

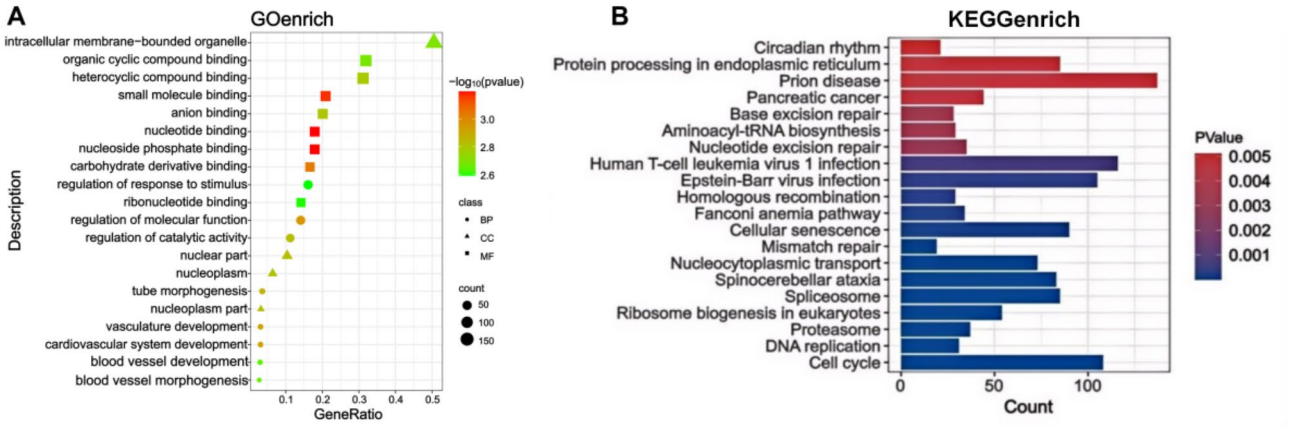

Fig. 3 Functional analysis of DEGs in PLCs under different oxygen conditions
(**A**) GO enrichment analysis of DEGs was performed, with colors representing varying p-value levels, transitioning from red (low) to green (high). The circle size reflects the number of DEGs, ranging from small (fewer) to large (more). A larger rich factor indicates a higher degree of GO enrichment. (**B**) KEGG enrichment analysis of DEGs was carried out, where the x-axis represents the enrichment count. The circle size corresponds to the number of enriched genes, and the color denotes the enrichment level. Higher enrichment scores, associated with lower P values, suggest a significant enrichment of differentially expressed genes in the relevant pathways. Similar methods were applied for subsequent analyses.

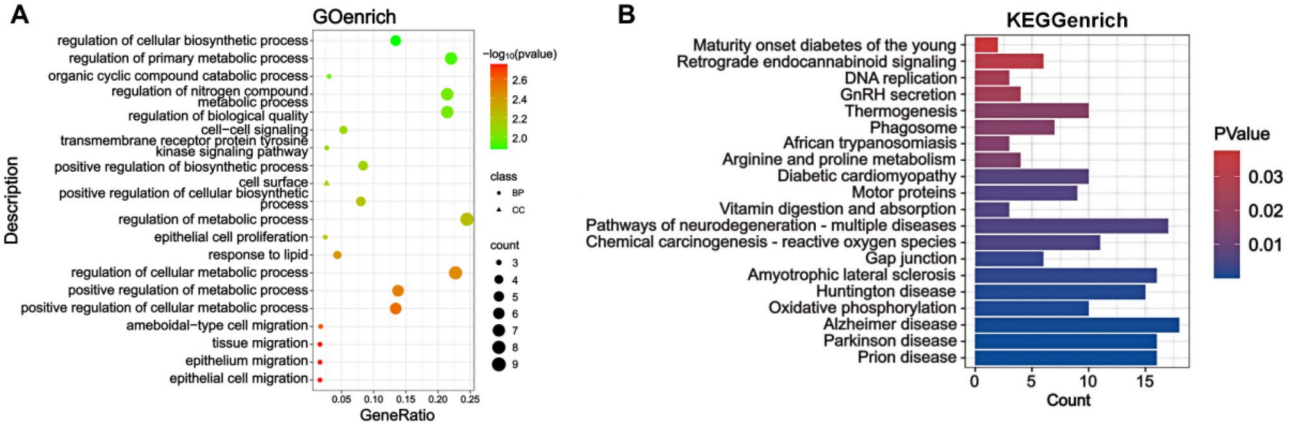

Fig. 4 Functional analysis of DEGs in PLCs by RDP under hypoxia
(**A**) GO enrichment analysis of DEGs. (**B**) KEGG enrichment analysis of DEGs

activation [34]. *SGK2* promotes cell proliferation, especially during stress responses and metabolic processes [35]. *SPP1* (osteopontin), a protein with multiple biological functions, promotes the proliferation of angiogenic progenitor cells through the PI3K/AKT signaling pathway [36]. The dual modulation of TNF and PI3K/AKT pathways by RDP creates a synergistic effect that enhances the protective properties of PLCs. This interaction is particularly evident in energy metabolism, where RDP not only upregulates signaling molecules but also supports their functional integration through feedback mechanisms. For instance, increased ATP levels, resulting from enhanced oxidative phosphorylation, can further stabilize and activate downstream targets within both pathways.

The synergistic effects of RDP on TNF and PI3K/AKT pathways are primarily mediated through enhanced mitochondrial function and energy metabolism. RDP upregulates key components of the electron transport chain, including *ATP5I*, *CYTB*, and COX complexes, leading to increased ATP production through oxidative phosphorylation. This enhanced energy status, in turn, facilitates the activation and stabilization of downstream effectors in both signaling pathways. Extensive research has established that mitochondrial Complexes I and III serve as primary ROS generation sites, exhibiting heightened vulnerability to oxidative damage [37]. Within Complex III, *CYTB* (cytochrome b) functions as the predominant source of mitochondrial ROS [38], with its upregulation demonstrating significant ROS-suppressive effects [39]. The electron transport chain component cytochrome c oxidase (*COX1*/*COX2*) catalyzes the terminal electron transfer reaction, facilitating cytochrome c oxidation and oxygen reduction to water [40]. Notably,

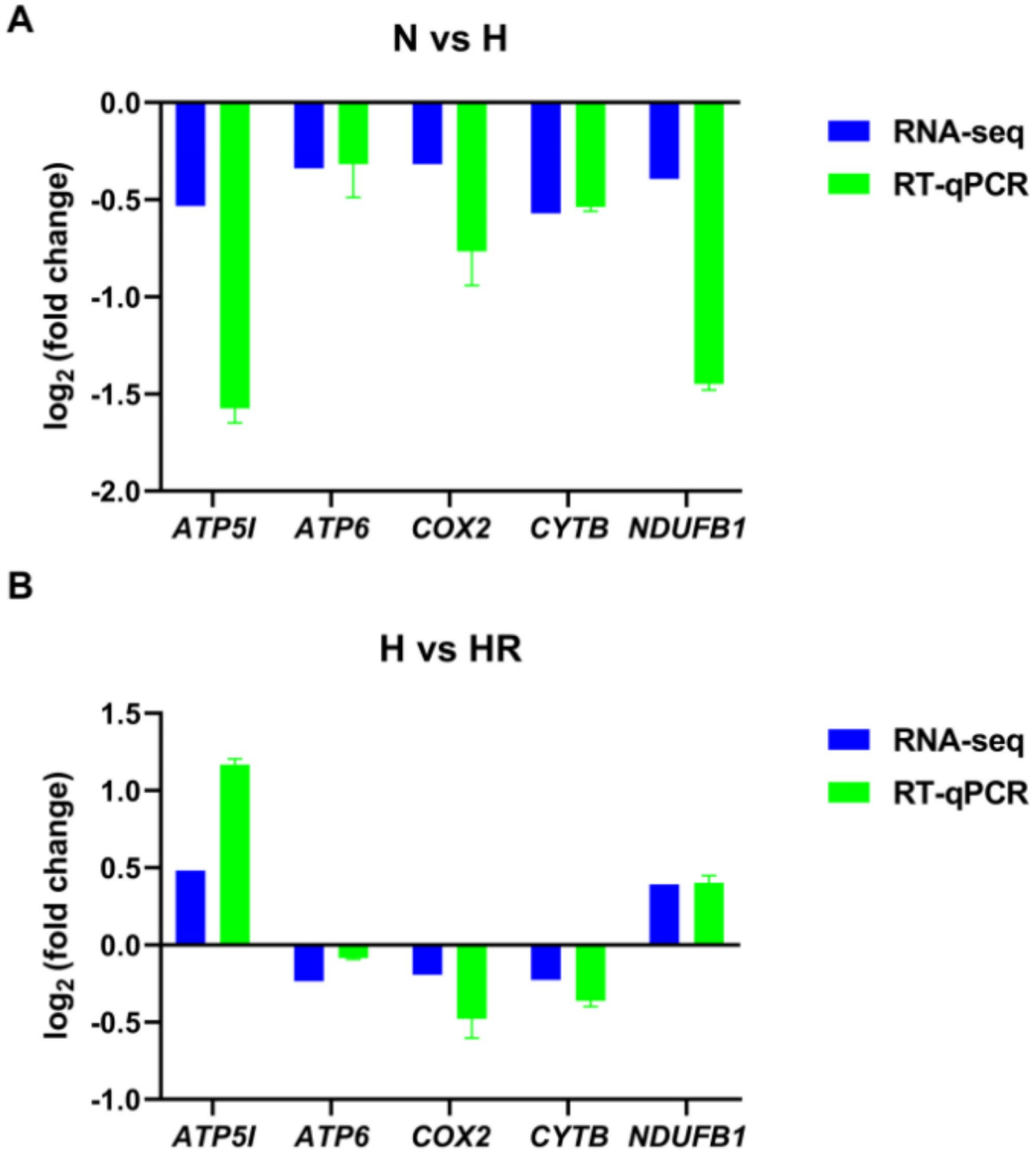

Fig. 5 Validation of the DEGs by qRT-PCR
(**A**) qRT-PCR results between N and H group. (**B**) qRT-PCR results between H and HR group

COX2 inhibition confers enhanced mitochondrial oxidative stress resistance while attenuating inflammatory responses [41]. *ATP5I*, an essential membrane subunit of ATP synthase (Complex V), plays a critical role in oxidative phosphorylation and maintenance of mitochondrial homeostasis [42]. Notably, the increased *ATP5I* expression and subsequent ATP production provide the energetic foundation for cellular protective mechanisms, while the modulation of *CYTB* and COX expression helps maintain redox homeostasis by regulating ROS production. This coordinated regulation of energy metabolism

and signaling pathways underlies RDP's protective effects on PLCs under oxidative stress.

Based on these findings, we conclude that RDP inhibits PLCs apoptosis and promotes cell proliferation primarily through up-regulating gene expression within the PI3K/AKT and TNF signaling pathways. The comprehensive modulation of these pathways provides a robust protective mechanism for PLCs under oxidative stress.

Conclusions

Hypoxia primarily inhibits cell proliferation by affecting signaling pathways such as cell cycle. RDP inhibits PLCs apoptosis and promotes cell proliferation by upregulating the expression of *CXCL2*, *JUNB* and *VCAM1* of the TNF signaling pathway, and *VEGFA*, *SGK2* and *SPP1* of the PI3K/AKT signaling pathway. This study offers a transcriptomic reference for RDP's protective role against hypoxia-induced inflammatory damage in PLCs and establishes a foundation for identifying relevant biomarkers.

Materials and methods

Cell culture

PLCs were sourced from Otwo Biotech Inc. (Guangzhou, China). The cells were cultured in DMEM-F12 medium containing 10% fetal bovine serum (FBS; GIBCO, Shanghai, China) and 1% penicillin (100 units/mL)/streptomycin (100 mg/mL) at 37 °C in a 5% CO_2 atmosphere, with medium changes every 24 h. Once the cells reached 80% confluence, they were trypsinized using 0.25% trypsin (Solarbio, Beijing, China) for passaging or further experimentation. The cells were assigned to three groups: the normal group (N), hypoxia group (H), and hypoxia + RDP group (HR). The N group was cultured under normal conditions without exposure to hypoxia or RDP treatment (Xi'an Qingzhi Biotechnology Co., Ltd., Xi'an, China). To induce hypoxia, the cells were placed in a Modular Incubator Chamber (Embrient Inc., USA) and exposed to a gas mixture of 1% oxygen (O_2), 5% carbon dioxide (CO_2), and 94% nitrogen (N_2) for 18 h. The HR group received RDP treatment (12.5 μg·mL^{-1}) for 18 h prior to hypoxia exposure [13].

CCK8 assay

For the Cell Counting Kit-8 (CCK8) assay (Biosharp, China), PLCs were plated in 96-well plates, with 1,500 cells per well. The cells were assigned to three groups: N group, H group, and HR group. Absorbance readings were taken at 450 nm using a microplate reader for each well to assess cell viability.

RNA-seq

The culture medium was discarded from the plate, and the cells were washed twice with PBS. RNA was then extracted from the cells using RNAiso Plus reagent (Takara Bio USA, Inc., USA). After isolating the total RNA, representative RNA samples were subjected to quality control (QC) and the RNA Integrity Number (RIN) score was assessed using an Agilent 2100 Bioanalyzer [43].

Transcriptome library preparation and sequencing were conducted on an Illumina NovaSeq 6000 system (Novogene Bioinformatics Technology Co., Ltd., Beijing, China). The raw sequencing data underwent quality control, including filtering out low-quality reads, checking for sequencing errors, and analyzing the GC content distribution.

Table 3 Primer information

Name	Sequence (5′-3′)	Length
ATP5I	F: GCCGCTATTCCGCCCTGTTC R: TTCTGCCAGTTCTCGCTCAATGC	149
ATP6	F: CACTAGCCCACTTTCTACCACAAGG R: AATAGGTGCCCTGCTGTAATGTTGG	139
COX2	F: CGGAACCCTACTTGGCGATGATC R: GCTCCGATTATTAGCGGTACGAGTC	135
CYTB	F: CATTCTGAGGAGCTACGGTCATCAC R: TGGCAGGATAAAGTGAAAGGCGAAG	143
NDUFB1	F: GGTTCACCGCTGCCCTTGG R: TGGTCACGCACAATCTGAAGTACG	89
β-actin	F: GATCTGGCACCACACCTTCTACAAC R: TCATCTTCTCACGGTTGGCTTTGG	107

Differential expression analysis

The criteria for screening DEGs were set as P-value < 0.05 and|log2 Fold change| ≥ 1 [44]. GO enrichment analysis was performed on the genes in the identified gene set using Goatools (https://github.com/tanghaibao/GOatools). A P-value (FDR) < 0.05 indicated significant enrich ment of GO functions. The log2 Fold change represents the ratio of gene expression levels between the treatment and control groups, processed by the shrinkage model in the difference analysis software, followed by taking the log base 2. For KEGG enrichment analysis, the R package "clusterProfiler" (v4.2.1, https://www.r-project.org) was used to create a script for gene set analysis, with calculation and visualization methods aligned with those used in GO enrichment analysis.

Real-time fluorescence quantitative validation

To verify the sequencing results and data analysis, qRT-PCR was performed on five selected DEGs from PLCs, with β-actin serving as the reference gene. Primers for both the reference gene and DEGs were designed and synthesized based on NCBI sequence information by Sangon Biotechnology Co., Ltd (Shanghai, China), with details provided in Table 3. Total RNA was extracted from the PLCs samples using RNAiso Plus reagent, and the RNA concentration and purity were assessed using

a NanoDrop One (Thermo Fisher Scientific, Waltham, MA, United States). Reverse transcription and amplification were carried out using the TaKaRa PrimeScript™ RT reagent Kit with gDNA Eraser (Perfect Real Time) (Takara Bio USA, Inc., USA). Thermo Fisher 7500 Fast Real-Time PCR system was used for real-time quantitative PCR measurement (Thermo Fisher Scientific, Waltham, MA, USA). The relative gene expression and fold change were calculated using the $2^{-\Delta\Delta Ct}$ method.

Data analysis

One-way ANOVA was performed using SPSS 26.0 statistical software, and multiple comparisons were performed using the LSD method, and $p < 0.05$ indicates significant difference, and $p > 0.05$ indicates no significant difference. Graph drawing and statistical analysis were performed with GraphPad Prism v.8.0.

Supplementary Information

The online version contains supplementary material available at https://doi.org/10.1186/s12917-025-04669-0.

Supplementary Material 1

Supplementary Material 2

Supplementary Material 3

Supplementary Material 4

Supplementary Material 5

Supplementary Material 6

Supplementary Material 7

Supplementary Material 8

Acknowledgements
Not applicable.

Author contributions
Jinting Luo: investigation, data curation, formal analysis, methodology, writing—original draft. Lei Wang: methodology, writing. Xuan Luo: methodology, writing. Jianbo Zhang: investigation, methodology. Tian Tian: writing—review and editing. Youli Yao: writing—review and editing. Dandan Luo: writing—review and editing. Guofang Wu: conceptualization, writing—review and editing, supervision. All authors have read and agreed to the published version of the manuscript.

Funding
This research was funded by the basic research project of Qinghai, grant number 2022-ZJ-752.

Data availability
Data is provided within the manuscript or supplementary information files.

Declarations

Ethics approval and consent to participate
Not applicable.

Consent for publication
All authors have read and agreed to the published version of the manuscript.

Competing interests
The authors declare no competing interests.

Received: 8 December 2024 / Accepted: 13 March 2025
Published online: 27 March 2025

References

1. Zhang CS, Liu Q, LiM, et al. RHOBTB3 promotes proteasomal degradation of HIFα through facilitating hydroxylation and suppresses the Warburg effect. Cell Res. 2015;25(9):1025–42.
2. Gianluca S, Giulia G, Anna C, et al. Hypoxia decreases ROS level in human fibroblasts. Int J Biochem Cell Biol. 2017;88:133–44.
3. Tönnies E, Trushina E, Oxidative Stress. Synaptic dysfunction, and Alzheimer's disease. J Alzheimers Dis. 2017;57(4):1105–21.
4. Ma YL, Zhang YP, Zhou J et al. Effects of simulated altitude hypoxia on the apoptosis of germ cells in rat. Chin J Birth Health Heredity. 2016(10):4.
5. Li X, Xu A, Li K, et al. CXCR4-SF1 bifunctional adipose-derived stem cells benefit for the treatment of Leydig cell dysfunction-related diseases. J Cell Mol Med. 2020;24(8):4633–45.
6. Chen KW, Zhao YJ, Wang L, et al. Transcriptome analysis of Porcine Leydig cells under different oxygen concentrations. China Anim Husb Veterinary Med. 2023;50(6):2185–95.
7. Guo T, Liu P, Wang Z et al. Luteolin binds streptolysin O toxin and inhibits its hemolytic effects and cytotoxicity. Front Pharmacol. 2022;(13):942180.
8. Na X, Fan FF, Jiang SY, et al. Rhodiola crenulate alleviates hypobaric hypoxia-induced brain injury via adjusting NF-κB/NLRP3-mediated inflammation. Phytomedicine. 2022;103(0):154240–154240.
9. Dennis Anheyer et al. Marleen Schröter,Gustav Dobos,. Traditional use of medicines from Rhodiola rosea (Roseroot). Zeitschrift für Phythotherapie. 2021;42 (6):280–291.
10. Egger P, Michele D'Ambrosio N, Aiello et al. Active constituents profiling of Rhodiola rosea L. Planta Med. 2007(9):0–0.
11. Li JT, Zhang PH, Qu XW, et al. Rhodiola polysaccharide effect on spermatogonial stem cell proliferation in vitro. Chin J Tissue Eng Res. 2016;20(10):1501–7.
12. Yu DD, Geng GX, Zhang CJ, et al. Effects of Rhodiola polysaccharides on proliferation of spermatogonial stem cells in vitro. J Domest Anim Ecol. 2013;34(7):54–7.
13. Luo JT, Xu FF, Wang L, et al. The effect of RSP on cell proliferation and apoptosis of Porcine Leydig cells with hypoxia. Acta Vet Et Zootechnica Sinica. 2024;55(6):2441–50.
14. Gianluca S, Giulia G, Francesca L, et al. Hypoxia and IF1 expression promote ROS decrease in cancer cells. Cells. 2018;7(7):64–64.
15. Li Cao, Juan W, Le B, et al. Effects of hypoxia on the growth and development of the fetal ovine hepatocytes in primary culture. PubMed. 2019;32(8):592–601.
16. Xu W, Mcarthur G. Cell cycle regulation and melanoma. Curr Oncol Rep. 2016;18(6):34.
17. Bele A, Mirza S, Zhang Y, et al. The cell cycle regulator ecdysoneless cooperates with H-Ras to promote oncogenic transformation of human mammary epithelial cells. Cell Cycle. 2015;14(7):990–1000.
18. Robert J, duronio, Yue X. Signaling pathways that control cell proliferation. Cold Spring Harb Perspect Biol. 2013;5(3):a008904–008904.
19. Maiso P, Huynh D, Moschetta M, et al. Metabolic signature identifies novel targets for drug resistance in multiple myeloma. Cancer Res. 2015;75(10):2071–82.
20. Ortmann B, Druker J, Rocha S. Cell cycle progression in response to oxygen levels. Cell Mol Life Sci. 2014;71(18):3569–82.
21. Barbara B, Lieven DV. Transcriptional control of the cell cycle. Curr Opin Plant Biol. 2009;12(5):599–605.
22. Souradeep B, Jessica G, Andrew W, Jones, et al. Core control principles of the eukaryotic cell cycle. Nature. 2022;607(7918):381–6.
23. Gan Z, Fang X, Yin C, et al. Extraction, purification, structural characterization, and bioactivities of the genus Rhodiola L. polysaccharides: A review. Int J Biol Macromol. 2024;276(1):133614.
24. Murat S, Dilek B, Meltem Ö, et al. Boric acid suppresses cell proliferation by TNF signaling pathway mediated apoptosis in SW-480 human colon cancer line. J Trace Elem Med Biol. 2022;71(1):126958–126958.
25. Liu L, Huang YX, Zhang KL, et al. Hepatitis B core antigen regulates dendritic cell proliferation and apoptosis through regulation of PKC/NF–κB signaling pathway. Mol Med Rep. 2018;18(6):5726–32.

26. Zhang R, Ye HW, Xin S, et al. Sortilin regulates keratinocyte proliferation and apoptosis through the PI3K-AKT signaling pathway. Life Sci. 2021;278(0):119630–119630.
27. Brownfoot FC, Hannan NJ, Cannon P, et al. Sulfasalazine reduces placental secretion of antiangiogenic factors, up-regulates the secretion of placental growth factor and rescues endothelial dysfunction. EBioMedicine. 2019;41:636–48.
28. Wang S, Shi M, Li J, et al. Endothelial cell-derived Exosomal circHIPK3 promotes the proliferation of vascular smooth muscle cells induced by high glucose via the miR-106a-5p/Foxo1/Vcam1 pathway. Aging. 2021;13(23):25241–55.
29. Cunha DA, Gurzov EN, Naamane N, et al. JunB protects β-cells from lipotoxicity via the XBP1-AKT pathway. Cell Death Differ. 2014;21(8):1313–24.
30. Selvaraj N, Budka JA, Ferris MW, et al. Extracellular signal-regulated kinase signaling regulates the opposing roles of JUN family transcription factors at ETS/AP-1 sites and in cell migration. Mol Cell Biol. 2015;35(1):88–100.
31. Cheng N, Kim KH, Lau LF. Senescent hepatic stellate cells promote liver regeneration through IL-6 and ligands of CXCR2. JCI Insight. 2022;7(14):e158207.
32. Ismail MB, Rajendran P, AbuZahra HM, et al. Mangiferin inhibits apoptosis in Doxorubicin-Induced vascular endothelial cells via the Nrf2 signaling pathway. Int J Mol Sci. 2021;22(8):null.
33. Wang M, Zhang J, Gong N. Role of the PI3K/Akt signaling pathway in liver ischemia reperfusion injury: a narrative review. Ann Palliat Med. 2022;11(2):806–17.
34. Zhang B, Qiangba Y, Shang P, et al. Gene expression of vascular endothelial growth factor A and hypoxic adaptation in Tibetan pig. J Anim Sci Biotechnol. 2016;7:21.
35. Wang H, Xu D, Toh MF, et al. Serum- and glucocorticoid-inducible kinase SGK2 regulates human organic anion transporters 4 via ubiquitin ligase Nedd4-2. Biochem Pharmacol. 2016;102:120–9.
36. Toru O, Tomomi U, Tetsuya N, et al. Osteopontin is a myosphere-derived secretory molecule that promotes angiogenic progenitor cell proliferation through the phosphoinositide 3-kinase/Akt pathway. Biochem Biophys Res Commun. 2007;359(2):341–7.
37. .Schwarzer M, Osterholt M, Lunkenbein A, et al. Mitochondrial reactive oxygen species production and respiratory complex activity in rats with pressure overload-induced heart failure. J Physiol. 2014;592(17):3767–82.
38. Moriggi M, Belloli S, Barbacini P, et al. Skeletal muscle proteomic profile revealed Gender-Related metabolic responses in a Diet-Induced obesity animal model. Int J Mol Sci. 2021;22(9):4680–4680.
39. Li H, Dai B, Fan J, et al. The different roles of miRNA-92a-2-5p and let-7b-5p in mitochondrial translation in Db/db mice. Mol Ther Nucleic Acids. 2019;17(1):424–35.
40. Li XJ, Dong L, Li A, et al. Butyrate ameliorates mitochondrial respiratory capacity of the Motor-Neuron-like cell line NSC34-G93A, a cellular model for ALS. Biomolecules. 2022;12(2):333–333.
41. Tarasenko N, Wilner HJ, Nudelman A, et al. Valproic acid prodrug affects selective markers, augments doxorubicin anticancer activity and attenuates its toxicity in a murine model of aggressive breast cancer. Pharmaceuticals (Basel). 2021;14(12):1244–1244.
42. Paumard P, Habersetzer J, Larrieu I, et al. Effect of mitochondrial ATP synthase subunit e and g (ATP5I and ATP5L) down-regulation in HeLa cells. BBA - Bioenergetics. 2014;1837(1):e18–9.
43. Schroeder A, Mueller O, Stocker S, et al. The RIN: an RNA integrity number for assigning integrity values to RNA measurements. BMC Mol Biol. 2006;7(1):3–3.
44. Love MI, Huber W, Anders S. Moderated Estimation of fold change and dispersion for RNA-seq data with DESeq2. Genome Biol. 2014;15(12):550–550.

Publisher's note